JACS Au
AN OPEN ACCESS JOURNAL OF THE AMERICAN CHEMICAL SOCIETY

pubs.acs.org/jacsau
Article

Substrate Conformational Switch Enables the Stereoselective Dimerization in P450 NascB: Insights from Molecular Dynamics Simulations and Quantum Mechanical/Molecular Mechanical Calculations

Published as part of JACS Au virtual special issue "Biocatalysis in Asia and Pacific".

Tai-Ping Zhou, Jianqiang Feng, Yongchao Wang, Shengying Li,* and Binju Wang*

Cite This: JACS Au 2024, 4, 1591−1604

Read Online

ACCESS | Metrics & More | Article Recommendations | Supporting Information

ABSTRACT: P450 NascB catalyzes the coupling of cyclo-(L-tryptophan-L-proline) (**1**) to generate (−)-naseseazine C (**2**) through intramolecular C−N bond formation and intermolecular C−C coupling. A thorough understanding of its catalytic mechanism is crucial for the engineering or design of P450-catalyzed C−N dimerization reactions. By employing MD simulations, QM/MM calculations, and enhanced sampling, we assessed various mechanisms from recent works. Our study demonstrates that the most favorable pathway entails the transfer of a hydrogen atom from N7−H to Cpd I. Subsequently, there is a conformational change in the substrate radical, shifting it from the Re-face to the Si-face of N7 in Substrate 1. The Si-face conformation of Substrate 1 is stabilized by the protein environment and the $\pi-\pi$ stacking interaction between the indole ring and heme porphyrin. The subsequent intermolecular C3−C6′ bond formation between Substrate 1 radical and Substrate 2 occurs via a radical attack mechanism. The conformational switch of the Substrate 1 radical not only lowers the barrier of the intermolecular C3−C6′ bond formation but also yields the correct stereoselectivity observed in experiments. In addition, we evaluated the reactivity of the ferric-superoxide species, showing it is not reactive enough to initiate the hydrogen atom abstraction from the indole NH group of the substrate. Our simulation provides a comprehensive mechanistic insight into how the P450 enzyme precisely controls both the intramolecular C−N cyclization and intermolecular C−C coupling. The current findings align with the available experimental data, emphasizing the pivotal role of substrate dynamics in governing P450 catalysis.

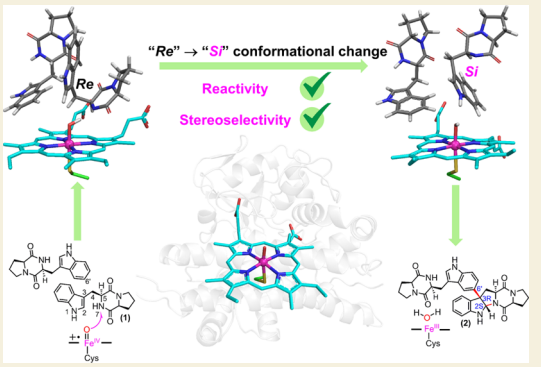

KEYWORDS: *P450, diketopiperazine, enzyme mechanisms, QM/MM, molecular dynamics, dimerization reaction, C−N bond formation*

1. INTRODUCTION

Small molecule natural products (NPs) can be valuable resources for treating a variety of diseases and disorders.[1−4] NPs consist of a large variety of compounds, including polyketides (PKs), nonribosomal peptides (NRPs), terpenoids, and alkaloids.[5−9] Among these, the tryptophan-linked dimeric diketopiperazine (DKP) derivatives possess distinctive structural architecture and extensive bioactive properties, such as anticancer, antitumor, antiviral, and neuroprotective activities.[10−14] Cytochrome P450s (CYPs),[15−23] a superfamily of heme-dependent enzymes, are demonstrated to be crucial for the biosynthesis of DKPs.[7,8,24−26] Recently, two homologous P450 enzymes (Scheme 1), NascB and NznB, have been characterized to catalyze the dimerization of cyclo-(L-tryptophan-L-proline) (**1**) to generate (−)-naseseazine C (**2**) and (+)-naseseazine B (**3**), respectively.[27−30] These types of transformations involve both the intramolecular C−N coupling and intermolecular C−C coupling, which are unique for the catalysis of P450s.[31−34]

In addition to NascB and NznB, another homologous enzyme named Nas_{F5053} has been characterized by Qu and co-workers.[28] Nas_{F5053} demonstrated high catalytic activity toward (**1**). Of note, the double mutant S284A-V288A predominantly produced compound (**2**). The high-resolution (1.68 Å) crystal structure of this mutant in complex with the native substrate (Figure 1) showed that the active site is occupied by two units of (**1**), with each occupying a distinct pocket. In addition, Substrate 1 is anchored by an array of H-bonding networks

Received: January 23, 2024
Revised: March 20, 2024
Accepted: March 21, 2024
Published: April 9, 2024

Scheme 1. Dimerization Reactions Catalyzed by NascB and NznB

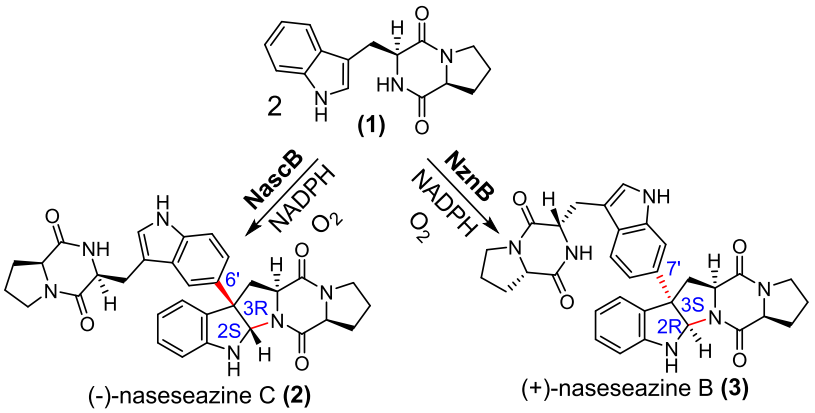

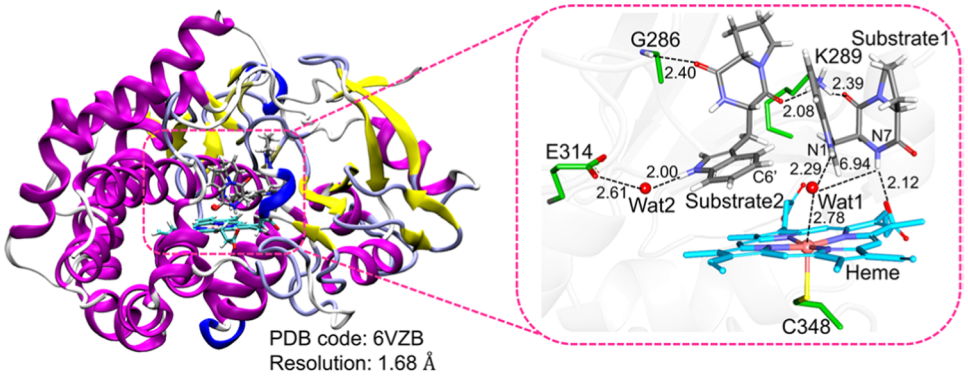

Figure 1. Crystal structure of Nas_{F5053} (PDB ID: 6VZB) in complex with two units of (**1**), and an enlarged view of the active site is displayed in the right box. Key hydrogen bonds are indicated by dashed lines. The distances are given in Å.

Scheme 2. Two Possible Dimerization Mechanisms in P450 NascB

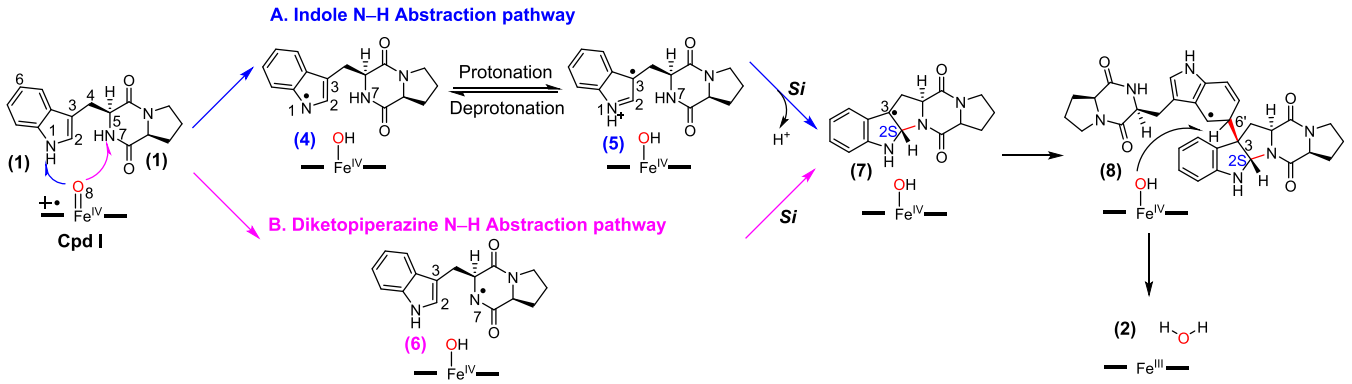

extended from residues K289, while Substrate 2 is stabilized by G286 and E314.

Scheme 2 summarizes two plausible mechanisms that emerge from experimental and computational investigations.[13,27,28] Based on structural information and the preliminary simulations, the catalytic route A has been proposed in Nas_{F5053} by Qu and co-workers.[28] In this route, the reaction is initiated by the hydrogen atom transfer (HAT) from the N1−H of Substrate 1 to Cpd I, the well-recognized active species in P450 catalysis.[35−40] This HAT step would afford an N1-centered indolyl radical intermediate (**4**), which may undergo further protonation to form a cation radical intermediate (**5**). This is followed by intramolecular C2−N7 coupling via a Mannich-type reaction, which could be coupled to the proton release from N7, leading to a pyrroloindoline radical intermediate (**7**) for the subsequent intermolecular C−C coupling reaction. Such a mechanism could be inferred from the structural information, indicating that the indole N1−H group of Substrate 1 is in the proximity of the heme-Fe, making it an ideal candidate for the HAT reaction (Figure 1). Furthermore, density functional theory (DFT) calculations indicated that the N1-centered radical resulting from HAT at N1 is significantly more stable than the N7-centered radical formed through HAT at the N7 site.[13,27] However, recent molecular dynamics (MD) investigations by Sherman and Houk showed that Substrate 1 may experience a conformational movement, leaving its N7−H close to Cpd I.[29] Additionally, the mechanism of the proton shuttle in route A

https://doi.org/10.1021/jacsau.4c00075
JACS Au 2024, 4, 1591−1604

remains elusive, as there are no apparent residues within the crystal structure that could mediate this process.[34] Therefore, there is still a lack of direct evidence supporting pathway A.

Sherman and co-workers have proposed mechanism B in NzeB based on DFT model calculations.[27] In this pathway, the reaction initiates with HAT from the N7−H group of Substrate 1, resulting in the formation of the diketopiperazyl radical (**6**). Unlike route A, intramolecular C2−N7 bond coupling within (**6**) may bypass the complicated proton shuttle. For the C2−N7 coupling, it was proposed that the N7 radical may attack the Si-face of the C2═C3 double bond, resulting in the correct configuration at the C2 site. This is followed by the intermolecular C3−C6′ bond formation via a radical mechanism. The subsequent rearomatization via the HAT from (**8**) intermediate to the ferry-hydroxo species (Cpd II) affords the final product (**2**). Interestingly, the crystal structure of NzeB (PDB ID: 6XAI) has been characterized, which bears quite similar active site architecture and substrate binding characteristics as those of Nas_{F5053}. Notably, the N1 of Substrate 1 is close to the heme-Fe (with a distance of 2.96 Å), while the N7 is 6.90 Å away from heme-Fe (Figure S1), indicating a preference for hydrogen atom abstraction (HAA) from the N1−H over the N7−H. However, the following MD study by the same group showed that the Substrate 1 repositioning may bring the N7−H group closer to the Cpd I species, thereby facilitating the generation of (**6**).[29]

Despite the aforementioned mechanistic insights, the molecular mechanism of the P450-catalyzed biosynthesis of DKPs is not fully elucidated, especially regarding the protein environment effects in dictating the regio- and stereoselective C−N and C−C coupling. Extensive studies have shown that the protein environment is key to the activity and selectivity of enzyme catalysis, while the neglect of such an effect in the QM model calculations may give biased descriptions of the kinetic and thermodynamic properties of enzymatic processes.[37,41−52] In this study, we reexamined the molecular mechanism of the P450 NascB with the combined MD simulations[53,54] and quantum mechanical/molecular mechanical (QM/MM) calculations.[55−59] Particularly, we systematically explored all conceivable catalytic pathways originating from two distinct binding modes of Substrate 1. Our multiscale calculations reveal that pathway B, which involves a conformational movement of the substrate radical, is the most favorable reaction pathway. Such a conformational switch of the substrate radical not only reduces the barrier of the intramolecular C−N bond coupling but also aligns with the correct stereoselectivity as observed in experiments.

2. METHODS

We used MD simulations for substrate binding conformational sampling. The hybrid QM/MM technique was employed to determine the catalytic mechanism. The umbrella sampling simulation was utilized to investigate the process of the conformational transformation. The details of these steps will be discussed in the following section, with the QM calculation method available in the Supporting Information.

2.1. System Setup and Classical MD Simulations

The initial structure coordinates of the enzyme−substrate complex were taken from the Protein Data Bank (PDB ID: 6VZB).[28] The missing residues were completed using the Modeller program.[60] In the previously suggested catalytic mechanism, the reaction is triggered by Cpd I species. The O atom above heme-iron was modeled as the oxo atom of Cpd I.[61,62] The protonation states of all titratable residues were assigned according to their pK_a values calculated by the PROPKA procedure.[63,64] Overall, all Glu and Asp residues were deprotonated, while the Arg and Lys residues were protonated. His109, His166, His177, His182, His205, and His 336 were protonated at the epsilon nitrogen, while His254, His262, His264, His316, His344, and His 381 were protonated at the delta nitrogen. The histidine residues His9, His188, and His194 were doubly protonated at both the epsilon and delta nitrogen atoms. The protonation states and local hydrogen-bonded networks were visually checked by using the VMD program.[65] The leap tools of the Amber package[66] were used to give the coordinates of the missing hydrogen atoms. For further MD simulations, the general Amber force field (GAFF)[67] was utilized for both substrates, whereas the partial atomic charges were received from the RESP method[68] at the B3LYP-D3BJ/6-31G(d,p)[69,70] level of theory. The AMBER ff14SB force field[71] was employed for the protein residues. The parameters of Cpd I were taken from a previous study,[72] while the force field parameters of Cpd II were prepared with the "MCPB.py" tool[73,74] of AmberTools18.[66] The parmchk2 tool from AmberTools18 was used to generate the missing parameters of the substrate. Several counter (sodium) ions were added to the protein surface with the leap tools to neutralize the total charge of the system. The resulting system was solvated in a rectangular box filled with the TIP3P[75] model waters extending up to a minimum distance of 16 Å from the enzyme's surface.

Using the above-prepared system, we started a consecutive two-step minimization of the targeted system to avoid steric clashes that occur during the system setup. In the first step, the added water molecules were subjected to minimization, while in the second step, the whole system was minimized using 10 000 steps of steepest descent and 10 000 steps of conjugate gradient algorithm, respectively. Then, the system was gently heated from 0 to 300 K under an NVT ensemble for 300 ps with a weak restraint of 25 kcal/mol/Å. To gain a uniform density after the heating process, 1.0 ns of density equilibration was performed under the NPT ensemble at a target temperature of 300 K and with a target pressure of 1.0 atm. The temperature value was kept using the Langevin thermostat[76] and the pressure was maintained with the Berendsen barostat[77] with a collision frequency of 2 ps and pressure relaxation time of 1 ps. This was followed by further equilibrations for 10 ns under an NPT ensemble without restraints for each system. Finally, three independent 200 ns productive MD simulations under the NPT ensemble were performed. The SHAKE method[78] was used to constrain the hydrogen bond while particle mesh Ewald and appropriate cutoff distances (∼10 Å) were used to treat the long-range electrostatic and van der Waals forces, respectively. All MD simulations were carried out with the GPU version of the AMBER 18 package.[66] The CPPTRAJ module of Amber 18 was used to analyze all of the results. The VMD software package was used for visualizing the MD simulation results.

2.2. QM/MM Calculations

All QM/MM calculations[55,56] were carried out using representative snapshots extracted from the MD simulation of the enzyme−substrate complexes. The representative snapshots were chosen based on the near-attack conformation from the MD trajectory (i.e., the shortest distance between the oxo of Cpd I and the target N−H). The ChemShell software package[57,79] was employed to perform all QM/MM calculations. This is done in combination with TURBOMOLE[80] for treating the QM zone and DL_POLY[81,82] for the MM region with the AMBER force field. The electronic embedding scheme[83] was implemented to incorporate the polarizing effect of the enzyme environment on the QM region. Hydrogen link atoms with the charge-shift model were applied to treat the QM/MM boundary. The QM/MM system contains all proteins, counterions, and solvation waters within 12 Å of the protein. A truncated heme-porphyrin ring and the proximal cysteine as $-SCH_3$ were incorporated in the QM zone (see Figure S2 for the QM zone). The active region during QM/MM calculations includes all of the residues and solvent molecules within a distance of 16 Å from the Fe center. During QM/MM geometry optimization, the QM region was treated with the hybrid UB3LYP density functional,[69] which was demonstrated to be practical

https://doi.org/10.1021/jacsau.4c00075
JACS Au 2024, 4, 1591−1604

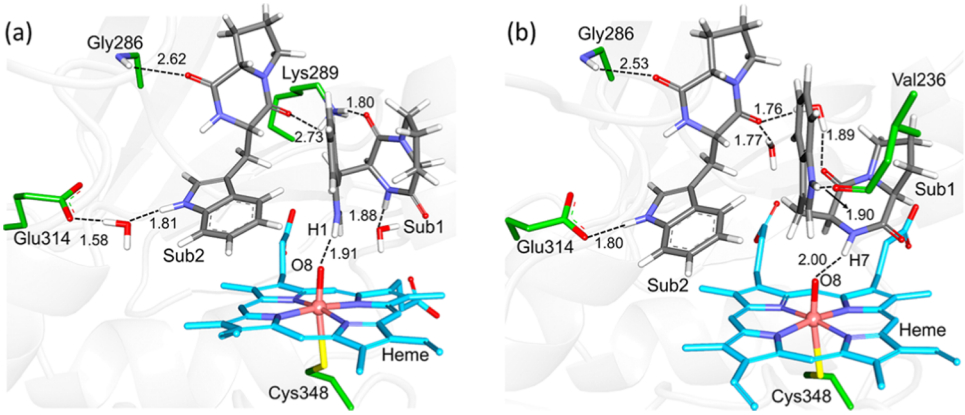

Figure 2. QM(UB3LYP-D3BJ/B1)/MM-optimized active site structure of Cpd I with the substrate for (a) Conf-a and (b) Conf-b. For the sake of clarity, unimportant hydrogen atoms are not shown. Key hydrogen bonds are indicated by dashed lines. The distances are given in Å.

for the study of P450 systems.[37,45,84−88] For geometry optimization and scanning calculations, the def2-SVP basis set[89] (labeled B1) was used. Then, the single-point calculations were conducted with the higher basis set def2-TZVP (labeled B2). The initial transition state (TS) structures were taken from the highest point of the potential energy surface (PES). Then, the TS was fully optimized using the dimer optimizer[90] implemented in the DL-FIND code.[91] The natural bond orbital (NBO) spin population[80] was obtained at the UB3LYP/B2 level. The Grimme DFT-D3BJ corrections[70] were added to all QM/MM calculations.[92−94] As both our calculations (refer to Tables S2 and S3) and previous studies show that S = 1/2 (doublet) and S = 3/2 (quartet) states exhibit generally similar reactivities for the Cpd I-mediated reactions,[37,95−98] our discussions are limited to the doublet state in the main text. The calculated spin populations of key atoms of the involved species are shown in Table S1.

2.3. Umbrella Sampling

The umbrella sampling[99] was applied to investigate the "Re → Si" conformational switch of the Substrate 1 radical species. The C2−C3−C4−C5 dihedral angle was chosen as the collective variable (CV) for the "Re → Si" transformation, which varies from −90.6 to 110.4, with a 3° interval for two adjacent windows. For each window, a 10 ns MD simulation with a basing harmonic potential (with a force constant of 200 kcal/mol/Å) was carried out to ensure sufficient overlap between two adjacent windows. During all restraint MD simulations, the covalent bonds containing hydrogen were constrained using SHAKE, and an integration step of 1 fs was used. In the production runs, a dump frequency of 1 ps^{-1} of the value of CV was used to collect the data needed for the potential of mean force (PMF) analysis. PMF was constructed with the weighted histogram analysis method (WHAM),[100,101] using the CV data in the last 5 ns restraint production simulations of each window. Convergence was analyzed by comparing the resultant PMF with the one obtained from the CV data of the last 10 ns of restraint production. To verify the stability of the Si conformation obtained from the umbrella sampling, the structure from the umbrella sampling window (CV = 104.3°) was relaxed with 200 ns MD simulations without any restraints.

3. RESULTS AND DISCUSSION

3.1. Substrate Binding Modes

To identify the binding modes of the two substrates, three separate 200 ns MD simulations were conducted (refer to Figures S3−S5). In line with the previous study, we observed two representative binding modes of Substrate 1 (Sub1) during the MD simulations.[29] In the initial 70 ns MD simulations, Sub1 maintains a conformation where its indole N1−H is H-bonded to the Cpd I species (labeled as Conf-a), resembling the conformation observed in the crystal structure (Figure 2a).[102] However, the binding mode of Conf-a is relatively unstable and rapidly transforms into another conformation after 70 ns (labeled as Conf-b), in which the DKP N7−H forms a hydrogen bond with iron-oxo (Figure 2b). Inspection of Figure 2a,b shows that the binding modes of Substrate 2 (Sub2) undergo minor changes, while Sub1 repositions significantly after 70 ns MD. Notably, in Conf-a, Sub1 engages in hydrogen-bonding interactions with Lys289, whereas in Conf-b, Sub1 is stabilized through hydrogen-bonding interactions with Val236. As both binding modes were observed during the MD simulations, both of them were considered for subsequent mechanistic investigation.

3.2. Indole N−H Abstraction Pathway A

Initially, we explored the intricate reaction mechanism in pathway A (Scheme 2), where Sub1's oxidation occurs via H-abstraction from its indole N1−H bond by Cpd I. Figure 3

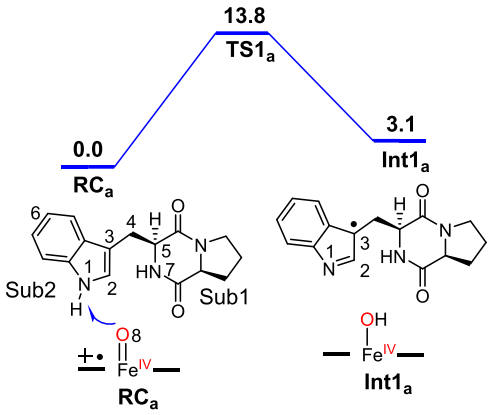

Figure 3. QM(UB3LYP/B2)/MM-calculated energy profile (in kcal/mol) for the H-abstraction from N1−H in pathway A, along with the schematic drawing of key intermediates.

depicts the QM/MM-calculated relative energy profile for pathway A, and the corresponding structures can be found in Figure S6. It is seen that the HAA from the indole NH group by Cpd I involves a low barrier of 13.8 kcal/mol, resulting in the intermediate $Int1_a$, whose energy is 3.1 kcal/mol higher than that of RC_a. Population analysis reveals that the radical is delocalized across the indole ring of Sub1 in $Int1_a$, with a significant population at C3 (−0.43) and N1 (−0.22). Commencing from the $Int1_a$ intermediate, we explored four

https://doi.org/10.1021/jacsau.4c00075
JACS Au 2024, 4, 1591−1604

Scheme 3. QM(UB3LYP/B2)/MM Calculated the Energy Barriers for All Possible Reaction Routes Emerging from Int1$_a$[a]

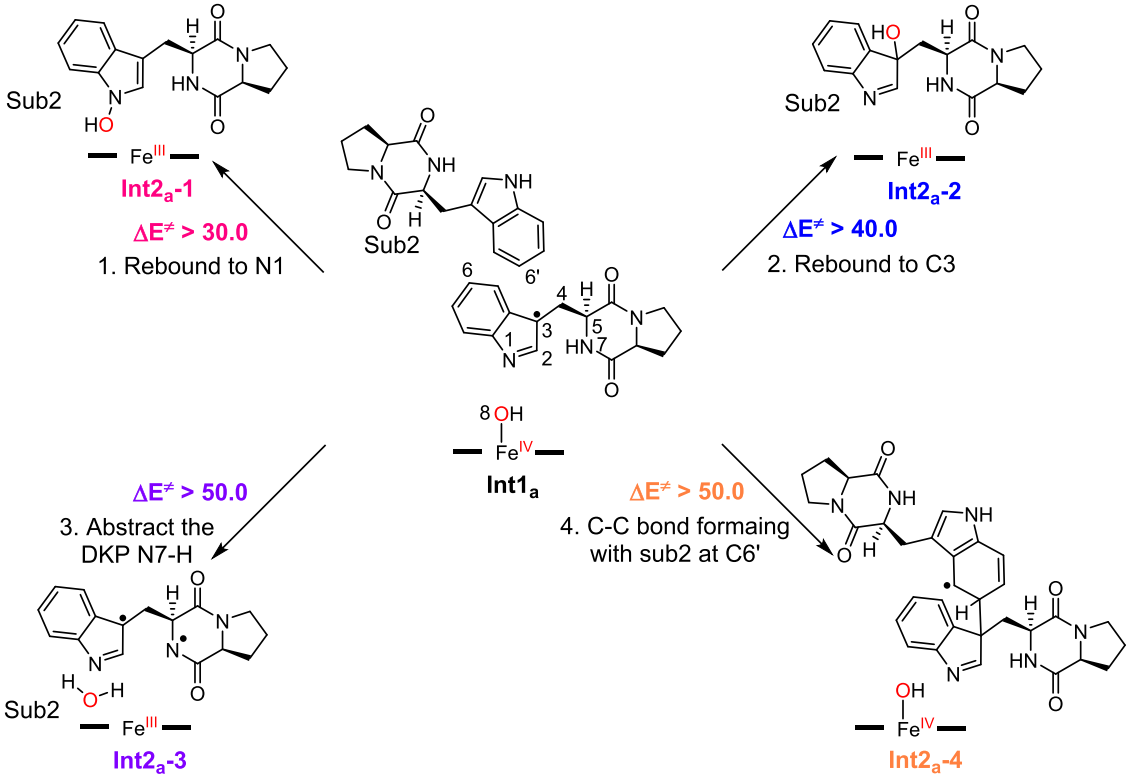

[a]Energies are given in kcal/mol relative to Int1$_a$.

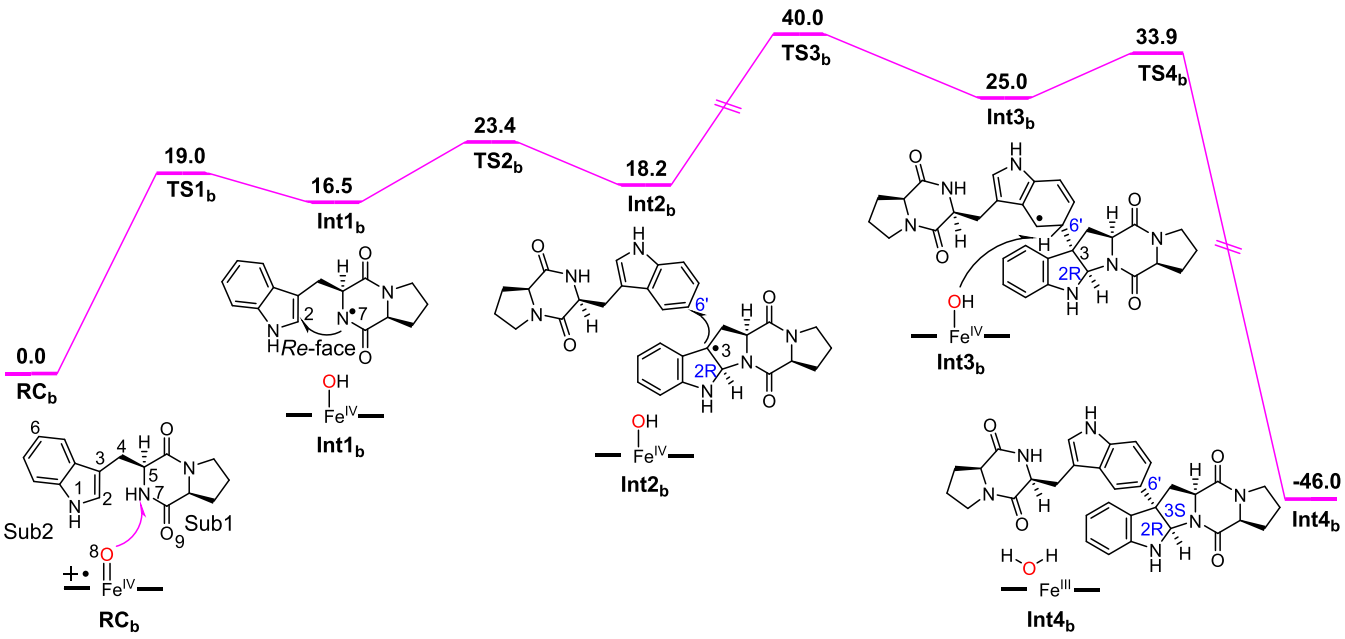

Figure 4. QM(UB3LYP-D3BJ/B2)/MM-calculated energy profile (in kcal/mol) for pathway B, along with a schematic drawing of key intermediates.

potential pathways, as outlined in Scheme 3. However, all of these pathways are kinetically inaccessible.

The first pathway involves the OH-rebound to the N1 site. However, its barrier is over 30.0 kcal/mol (Figure S7) and thus can be ruled out. In the second pathway, the OH-rebound to the C3 site also requires a high barrier of over 40.0 kcal/mol, mainly due to unfavorable substrate positioning (Figure S8). In the third route, Fe^{IV}−OH species in Int1$_a$ may perform HAA from the N7−H site, transforming the indolyl radical to a diradical species. However, this route requires a remarkable barrier of more than 50.0 kcal/mol (Figure S9). In the fourth route, we investigated the intermolecular C3−C6′ bond formation between the indolyl radical and Sub2, but the process experiences a barrier of over 50.0 kcal/mol according

https://doi.org/10.1021/jacsau.4c00075
JACS Au 2024, 4, 1591−1604

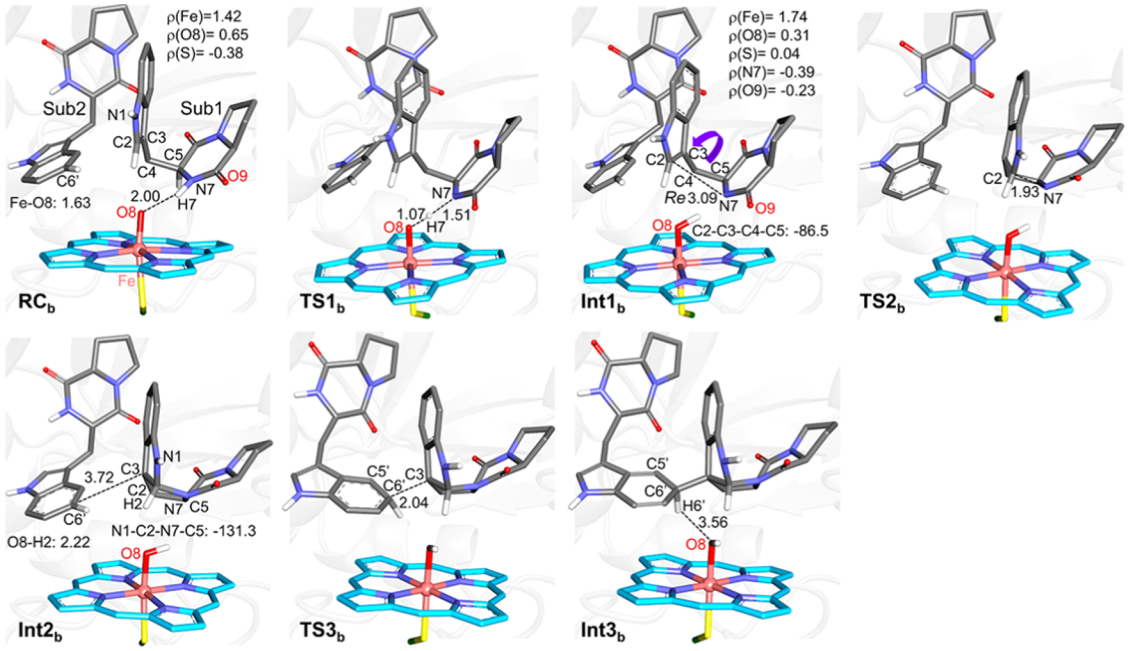

Figure 5. QM(UB3LYP-D3BJ/B1)/MM-obtained structures of key species along pathway B, shown along with the spin population of the key atoms. The distances are given in Å. For clarity, only relevant hydrogen atoms are shown.

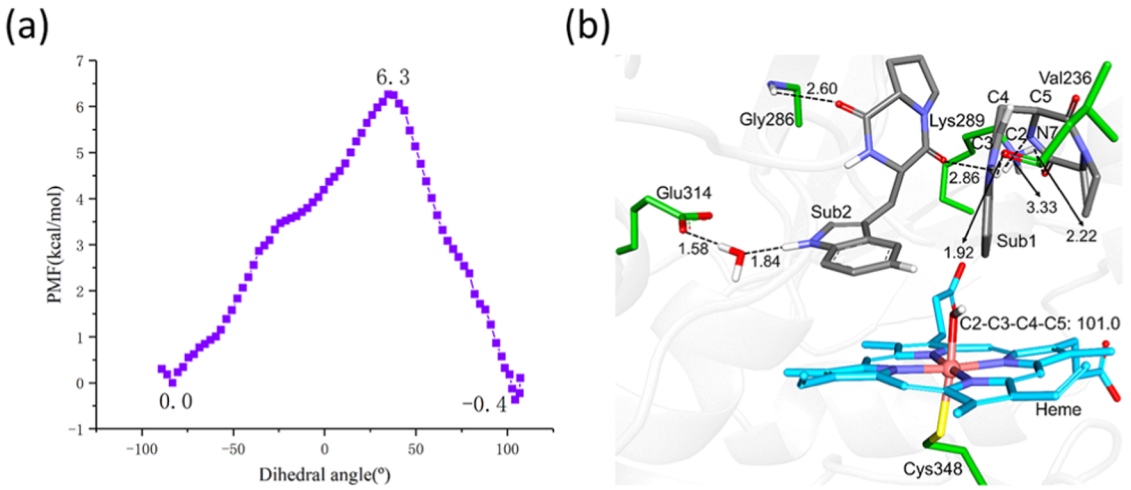

Figure 6. (a) Calculated PMF (in kcal/mol) for the transformation of "Re" conformation to "Si" conformation. The reaction coordinate is defined as the C2−C3−C4−C5 dihedral angle. (b) The active site structure of the "Si" conformation. For clarity, unimportant hydrogen atoms are not shown. Key hydrogen bonds are indicated by dashed lines. The distances are given in Å.

to our scanned energy profile (Figure S10). Obviously, the HAA from the substrate N1−H group would afford dead-end intermediate Int1$_a$ that cannot undergo further transformations.

Beginning with the Int1$_a$ intermediate, the protonation of the indolyl radical species, as suggested by Qu et al., yields a protonated species.[28] To verify its possibility, we conducted further testing using the QM method. The pK_a of indole radical species is approximately 4.8 lower than that of the experimental environment (∼7.5, Scheme S1),[103] indicating that the protonation of the Sub1 radical is endothermic of 6.55 kcal/mol[104] (estimated by 4.8 × 1.364 kcal/mol), making it thermodynamically unfavorable. QM calculations show that the protonated indolyl radical presents a high energy barrier in all assessed reactions (Scheme S1, Figure S11). In summary, all of our calculations suggest that pathway A in Scheme 2 is highly unfavorable and thus can be ruled out.

3.3. Diketopiperazine N−H Abstraction Pathway B

In this section, we proceed to investigate the dimerization reactions from the binding conformation of Conf-b. As shown in Figure 2b, the H7 atom of Sub1 forms a hydrogen bond with Fe^{IV}═O in Conf-b, implying that the Fe^{IV}═O species might catalyze HAA from the N7 bond. Figure 4 presents the QM/MM-calculated energy profiles initiated from HAA from the N7−H group (pathway B). The primarily QM/MM-optimized structures involved in the reactions are depicted in Figure 5. It is observed that HAA from the N7−H bond experiences an energy barrier of 19.0 kcal/mol, leading to the intermediate Int1$_b$, which is 16.5 kcal/mol higher than RC$_b$. The spin population analysis shows that one electron transfers from Sub1 to the porphyrin group during H-abstraction by

https://doi.org/10.1021/jacsau.4c00075
JACS Au 2024, 4, 1591−1604

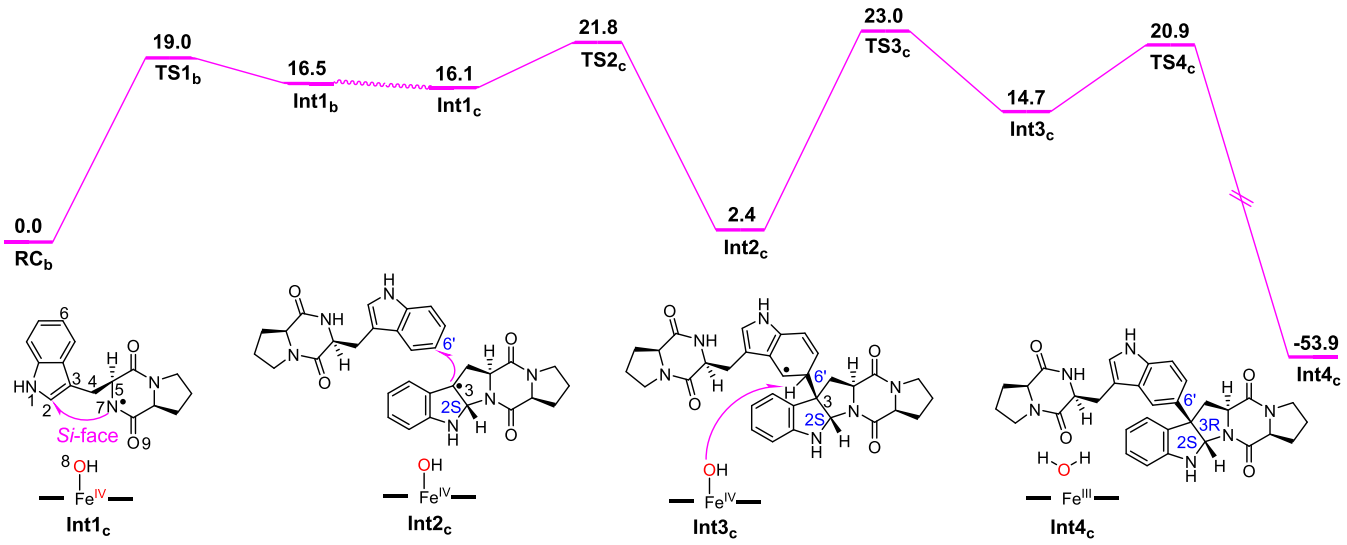

Figure 7. QM(UB3LYP-D3BJ/B2)/MM-calculated energy profile (kcal/mol) for pathway B after the conformational transformation of the Sub1 radical, along with the schematic drawing of the key intermediates.

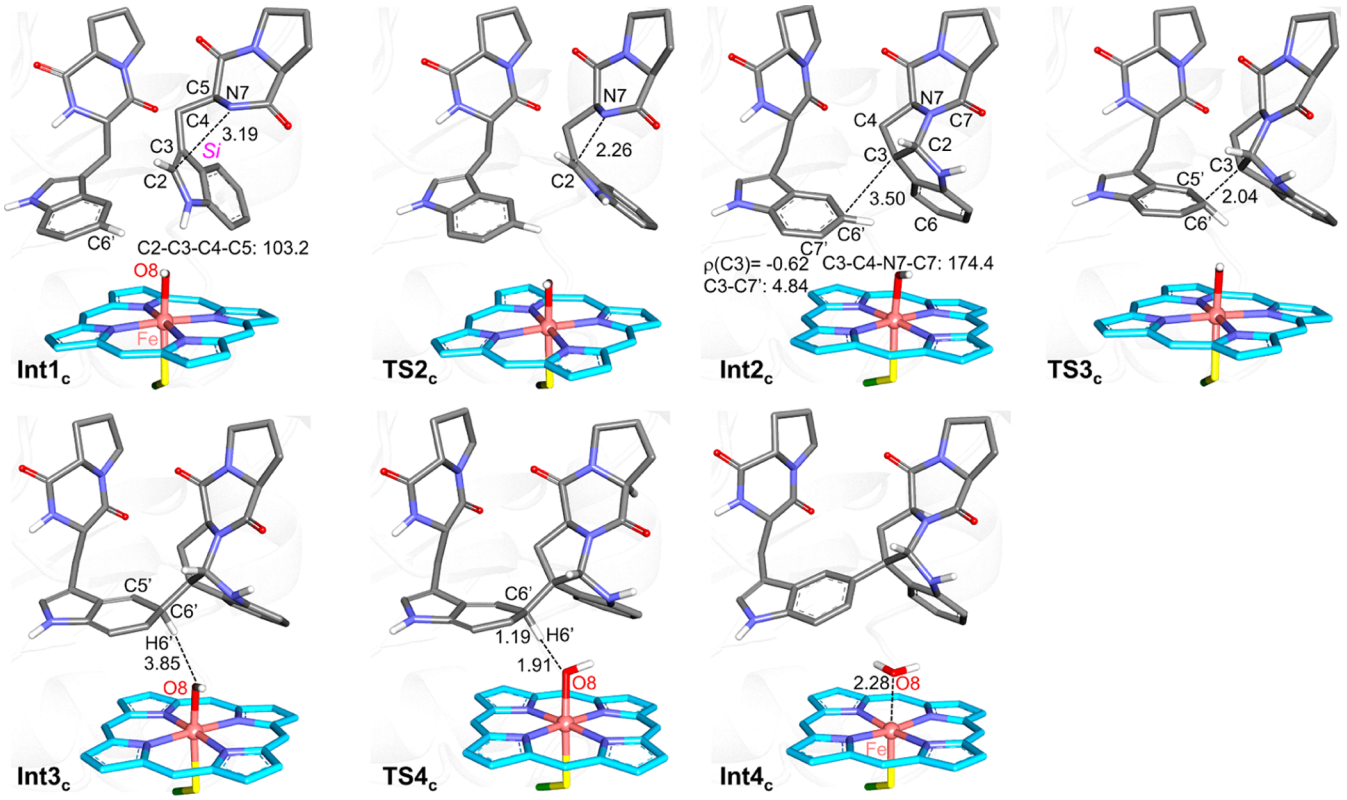

Figure 8. QM(UB3LYP-D3BJ/B1)/MM-obtained structures of key species along pathway B after the conformational transformation of the Sub1 radical are shown along with the spin population of key atoms. The distances are given in Å. For clarity, only relevant hydrogen atoms are shown.

Fe^{IV}═O species (Figures 5 and S12), leading to the Fe(IV)−OH state in the so-formed $Int1_b$. This finding is consistent with earlier studies.[13,27] Starting from $Int1_b$, we first investigated the attack of N7 onto the C2 site of the indole ring via the Re-face direction, which may afford the pyrroloindoline radical intermediate. As depicted in Figure 4, the calculated barrier for this step is 23.4 kcal/mol relative to RC_b. However, we found that C2 maintains the *R* configuration in the resulting $Int2_b$. Starting from $Int2_b$, we further investigated the intermolecular C3−C6′ coupling between the pyrroloindoline radical and the Sub2. As shown in Figure 4, the process requires a quite high barrier of 40.0 kcal/mol relative to that of RC_b. Since the C2−H bond is close to the Fe^{IV}−OH species in $Int2_b$, we also investigated the HAT from the C2−H to the Fe^{IV}−OH species, and the process requires a relatively high barrier of 25.6 kcal/mol compared to RC_b (Figure S13). All of these observations indicate that the direct intramolecular C2−N7 coupling within $Int1_b$ may not be responsible for the dimerization reactions.

https://doi.org/10.1021/jacsau.4c00075
JACS Au 2024, 4, 1591−1604

Inspired by our previous study, we assume the diketopiperazyl radical may adopt the flexible conformation.[45,105−107] Consequently, we have explored the rotation of the dihedral angle C2−C3−C4−C5 using the enhanced umbrella sampling.[108−111] As indicated in Figure 6a, the rotation of the C2−C3−C4−C5 dihedral angle experiences a barrier of 6.3 kcal/mol, leading to another stable conformation that is 0.4 kcal/mol lower than the initial conformation. In the new conformation, the Sub1 radical is stabilized by hydrogen-bonding interactions with surrounding residues, such as Val236 and Lys289 (Figure 6b). In addition, the dihedral angle has increased to 101.0°, which may enable N7 to attack the C2 of indole via the "Si" conformation, leading to the *S* configuration at the C2 site in the formed pyrroloindoline radical intermediate. To further verify the stability of the Sub1 radical in its "Si" conformation, we have performed 200 ns fully relaxed MD simulations, showing that the system is quite stable, with an RMSD value of less than 1.5 Å (Figure S16a). The analysis[112] of protein−ligand interaction for both "Re" and "Si" conformation revealed that the diketopiperazyl radical was stabilized by nonbonding interactions including hydrogen bond, hydrophobic interaction, and $\pi-\pi$ stacking (Table S5). In addition, the nonbonding interaction between the Sub1 radical and the protein environment was calculated to be −53.5 kcal/mol in the "Si" conformation, which is comparable to the value of −55.1 kcal/mol in the "Re" conformation (Figure S17), supporting the idea that both conformations of the radical species can be stabilized by the protein environment. In comparison, we also investigated the conformational change of substrate 1 before the H-abstraction reaction. However, the conformational transformation of substrate 1 was found to be unfavorable thermodynamically in both binding modes (Conf-a and Conf-b; see Figure S18). Thus, the generation of the radical species via the H-abstraction facilitates the conformational transformation of Sub1.

Figure 7 presents the QM/MM-calculated relative energy profile for the dimerization reactions initiated from the "Si" conformation of the Sub1 radical, while Figure 8 illustrates the QM/MM-optimized structures of key intermediates and TSs. In $Int1_c$, the spin population predominantly resides on the N7 atom (−0.69). Starting in $Int1_c$, the N7 attacks the Si-face of the C2═C3 bond ($Int1_c \rightarrow TS2_c$), which involves a barrier of 21.8 kcal/mol that forms $Int2_c$ and affords $Int2_c$ that is 2.4 kcal/mol higher in energy than RC_b. In $TS2_c$, the C2−N7 bond distance has shortened to 2.26 Å, compared to 3.19 Å in $Int1_c$. In the nascent $Int2_c$, the C3 site carries the most spin population (−0.62), which would facilitate the following intermolecular C3−C6′ bond coupling between the $Int2_c$ radical and Sub2 via a radical-mediated process. This process involves an energy barrier of 23.0 kcal/mol relative to RC_b, leading to $Int3_c$, which is 14.7 kcal/mol higher than RC_b. In comparison, the calculated barrier of C3−C7′ bond coupling is 30.7 kcal/mol (Figure S19), which is in line with experiments in which the C3−C6′ coupling is favored over that of the C3−C7′ coupling. This is mainly attributed to the shorter distance of C3−C6′ (3.50 Å) relative to that of C3−C7′ (4.84 Å), suggesting that the substrate positioning is key to the selective C3−C6′ bond formation. Therefore, our calculations support that the C−C bond formation occurs via a radical-mediated mechanism, rather than a cationic Friedel−Crafts mechanism suggested before.[34] In the final step, the HAT from C6′−H to Cpd II forms the aromatization product ($Int3_c \rightarrow Int4_c$), which involves an energy barrier of 20.9 kcal/mol relative to RC_b.

Inspection of Figures 5 and 8 shows that the intermolecular C3−C6′ bond coupling from the "Si" conformation ($Int2_c \rightarrow TS3_c$ in Figure 7) is remarkably favored over that from the "Re" conformation ($Int2_b \rightarrow TS3_b$ in Figure 4). This is primarily because $Int2_c$ has a significantly lower energy compared to $Int2_b$. In $Int2_b$, dihedral N1−C2−N7−C5 features an angle of −131.3°, which leads to significant ring strain in the newly formed five-membered ring. In contrast to $Int2_b$, the ring strain is significantly released in $Int2_c$, attributed to the dihedral angle C3−C4−N7−C7 measuring 174.4°. Moreover, the existence of intermolecular $\pi-\pi$ stacking interactions (Figure S20) between the indole ring and porphyrin contributes to the additional stabilization of $Int2_c$. Consequently, the rotation of the C2−C3−C4−C5 dihedral angle not only diminishes the barrier for the intermolecular C3−C6′ bond coupling between pyrroloindoline radical intermediate and Sub2 but also leads to the correct stereoselectivity for the dimerization reaction.

3.4. Why the O-Substituted Substrate Is Not Reactive for Dimerization Reaction

In an experiment conducted by Qu and co-workers, an O-substituted substrate (O-sub) analogue was tested, but no reactivity can be identified (Figure 9a).[13] As the analogue of

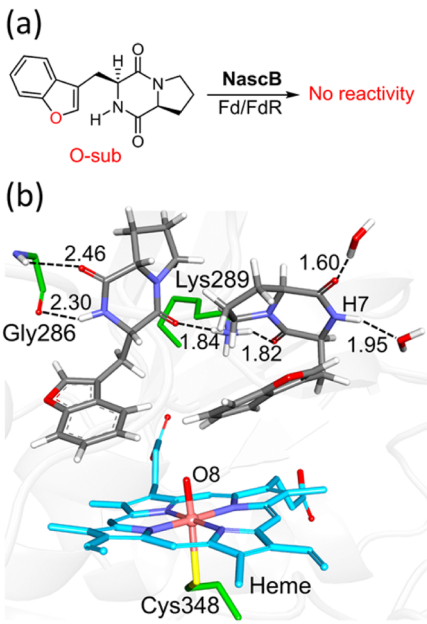

Figure 9. (a) O-substituted substrate (O-sub) analogue tested in NascB. (b) Representative structure of the Cpd I with the O-sub from MD simulation. For clarity, unimportant hydrogen atoms are not shown. Key hydrogen bonds are indicated by dashed lines. The distances are given in Å.

the O-sub does not undergo dimerization by NascB, it was assumed that the H-abstraction from the indole N−H could be key to the dimerization by NascB. To rationalize such experiment observation, we performed 200 ns MD simulations for the Cpd I state of P450 NascB with the O-sub. Our MD simulations demonstrate that the system can reach a stable convergence state after 60 ns, as evidenced by calculated RMSD (Figure S21a). In a snapshot from the converged trajectory, it is seen that the N7−H group of the O-sub is far away from Cpd I, with an average distance of ∼10 Å (Figure S21b). In addition, the substituted oxygen atoms of the O-sub

https://doi.org/10.1021/jacsau.4c00075
JACS Au 2024, 4, 1591−1604

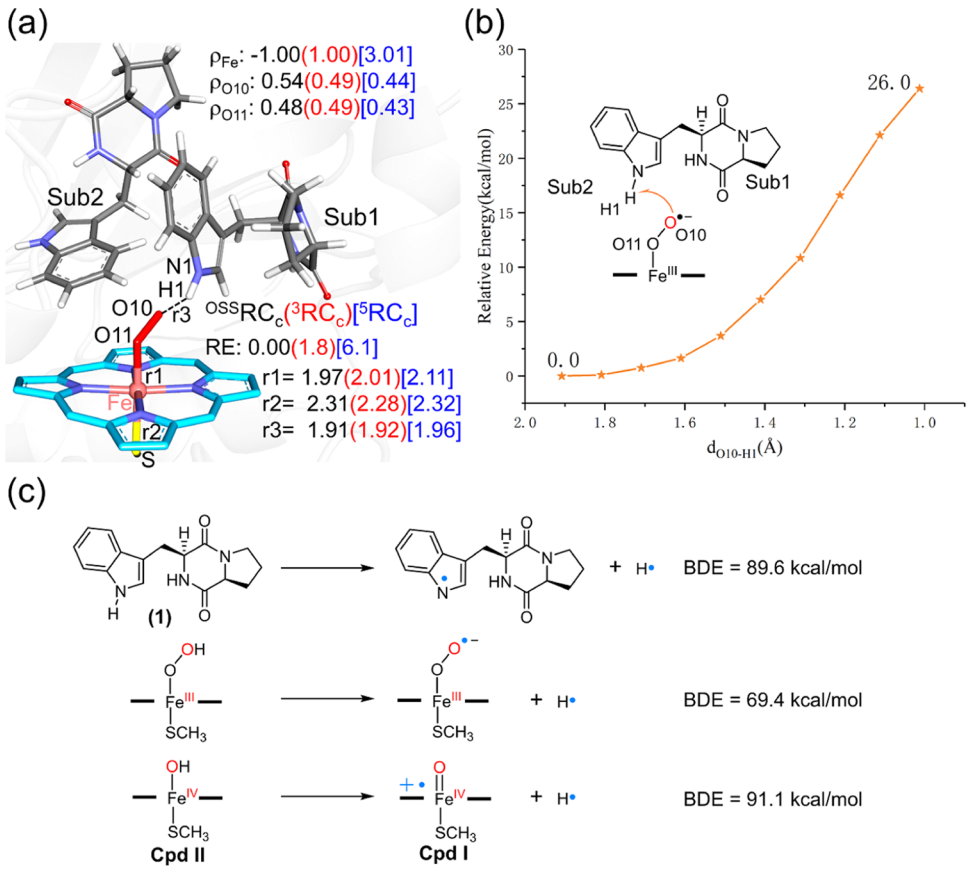

Figure 10. (a) QM(UB3LYP-D3/B1)/MM-optimized ferric-superoxide species in different spin states; the superscripts for OSS, 3, and 5 indicate the open-shell singlet, triplet, and quintet, respectively. The relative energies (RE) are given in kcal/mol and distances in angstroms. (b) QM(UB3LYP-D3/B1)/MM-scanned energy profile for the H-abstraction from $^{OSS}RC_c$. The reaction coordinate is defined as the O10−H1 distance. (c) The calculated BDE values of the N1−H1 bond of (**1**), the O−H bond of the Fe^{III}−OOH species, and the O−H bond of Cpd II.

do not form any hydrogen-bond interaction in the active center (Figure 9b). Consequently, our MD simulation results indicate that the inappropriate binding conformation of the O-substrate renders it highly unfavorable to initiate HAA from the N7−H group, potentially explaining why this substrate does not exhibit reactivity in the dimerization reaction.

3.5. Can Ferric-Superoxide Act as a Potential Oxidant in P450 NascB

In very recent research, the ferryl-intermediate was suggested as an oxidant to facilitate the dimerization of cyclic dipeptides by P450 AspB.[113] To verify if such an intermediate could be involved in the substrate dimerization in P450 NascB, we have conducted MD simulations and QM/MM calculations on the ferric-superoxide (Fe^{III}−$OO^{\bullet-}$)-mediated HAA from the indole N1−H of the substrate in the NascB enzyme. In line with a previous study,[114] the ground state is calculated to be the open-shell singlet (OSS), as summarized in Figure 10a. In the optimized $^{OSS}RC_c$ structure, the spin populations on the atoms of O10 and O11 are 0.54 and 0.48, respectively, while the spin population on Fe is −1.00. This is consistent with a typical OSS ferric-superoxide complex.[114] Further QM/MM scanning from the $^{OSS}RC_c$ structure shows that the energy of HAA from N1 increases steadily, with no stable intermediate that can be identified along the energy profile. Additionally, the estimated energy barrier exceeds 26.0 kcal/mol (Figure 10b). All of these findings indicate that the ferric-superoxide species lacks sufficient reactivity to initiate HAA from the substrate's indole NH group. Such finding is consistent with the previous study by Shaik and co-workers, in which the ferric-superoxide was demonstrated to be a sluggish oxidant for the C−H hydroxylation in $P450_{cam}$.[115] To further compare the different reactivity between the ferric-superoxide species and Cpd I species, we computed the bond dissociation energy (BDE) of the O−H bond in different species (Figure 10c).[116−119] It is seen that the BDE values of Cpd II are comparable to those of the substrate N−H bond. However, the BDE of Fe^{III}−OOH is 21.7 kcal/mol lower than that of the Cpd II, indicating the ferric-superoxide species has a much lower driving force to conduct HAA, compared to the Cpd I species.[120,121] We additionally explored whether ferric-superoxide is capable of initiating HAA from the DKP N7−H bond of the substrate (Figure S23a). However, this process requires a high barrier of over 29.9 kcal/mol (Figure S23b), mainly because the DKP N7−H bond is even stronger than that of the indole N1−H (Figure S23c).[27]

4. CONCLUSIONS

This study elucidates the molecular mechanism of the P450 NascB-catalyzed dimerization reaction through comprehensive multiscale calculations, as summarized in Scheme 4. The reaction is initiated from HAA from the DKP N7−H atom of Sub1, resulting in the formation of the N7-centered radical species. Subsequently, a pivotal conformational change of the Sub1 radical is necessary to position the N7 atom on the *Si*-face of the indole C2═C3 double bond. This is followed by intramolecular C2−N7 bond formation to generate a

https://doi.org/10.1021/jacsau.4c00075
JACS Au 2024, 4, 1591−1604

Scheme 4. QM/MM-Predicted Mechanism of Stereoselective Dimerization by P450 NascB in This Work

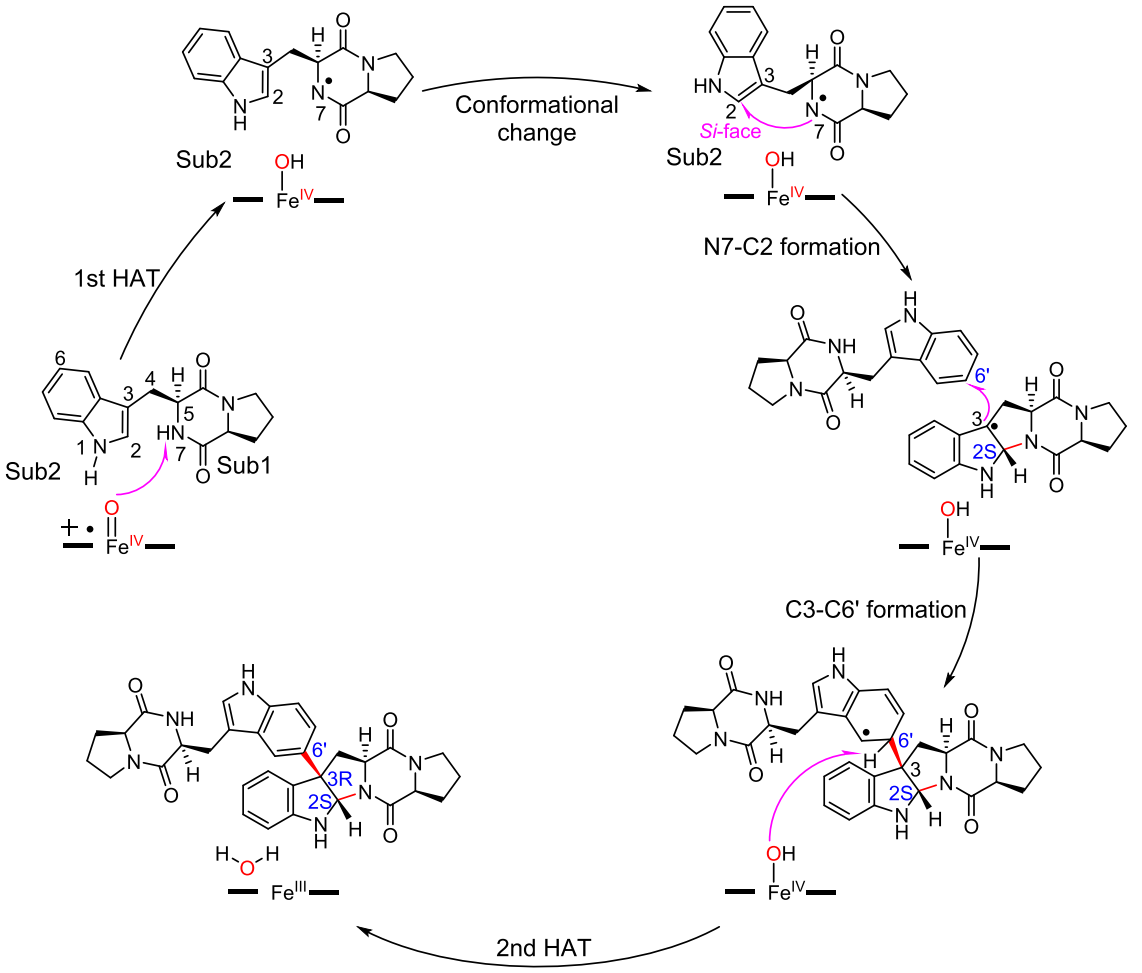

pyrroloindoline radical species. The subsequent intermolecular C3−C6′ bond formation was found to occur via a radical-mediated mechanism, instead of a cationic Friedel−Crafts mechanism. Importantly, the conformational switch of the Sub1 radical not only lowers the barrier of the intermolecular C3−C6′ bond formation but also affords the correct stereoselectivity as observed in experiments. Therefore, our study highlights that the conformational movement of the substrate, which is controlled by the protein environment, can be vital to P450-catalyzed dimerization reactions. We anticipate that these findings can aid our understanding of other P450-catalyzed dimerization reactions, such as intermolecular C−C coupling,[122−127] C−N coupling,[27,128,129] and C−S coupling.[130−133]

■ ASSOCIATED CONTENT

Supporting Information

The Supporting Information is available free of charge at https://pubs.acs.org/doi/10.1021/jacsau.4c00075.

Optimized structures; calculated spin densities; QM/MM energies; and the Cartesian coordinates of all computed species (PDF)

■ AUTHOR INFORMATION

Corresponding Authors

Shengying Li − *State Key Laboratory of Microbial Technology, Shandong University, Qingdao 266237, China;* orcid.org/0000-0002-5244-870X; Email: lishengying@sdu.edu.cn

Binju Wang − *State Key Laboratory of Physical Chemistry of Solid Surfaces and Fujian Provincial Key Laboratory of Theoretical and Computational Chemistry, College of Chemistry and Chemical Engineering, Xiamen University, Xiamen 361005, China;* orcid.org/0000-0002-3353-9411; Email: wangbinju2018@xmu.edu.cn

Authors

Tai-Ping Zhou − *State Key Laboratory of Physical Chemistry of Solid Surfaces and Fujian Provincial Key Laboratory of Theoretical and Computational Chemistry, College of Chemistry and Chemical Engineering, Xiamen University, Xiamen 361005, China*

Jianqiang Feng − *State Key Laboratory of Physical Chemistry of Solid Surfaces and Fujian Provincial Key Laboratory of Theoretical and Computational Chemistry, College of Chemistry and Chemical Engineering, Xiamen University, Xiamen 361005, China*

Yongchao Wang − *State Key Laboratory of Physical Chemistry of Solid Surfaces and Fujian Provincial Key Laboratory of Theoretical and Computational Chemistry,*

https://doi.org/10.1021/jacsau.4c00075
JACS Au 2024, 4, 1591−1604

College of Chemistry and Chemical Engineering, Xiamen University, Xiamen 361005, China

Complete contact information is available at: https://pubs.acs.org/10.1021/jacsau.4c00075

Notes

The authors declare no competing financial interest.

■ ACKNOWLEDGMENTS

This work was supported by the National Key Research and Development Program of China (no. 2019YFA0906400 to B.W.) and the National Natural Science Foundation of China (no. 22122305 and 22073077 to B.W. and no. 32025001 to S.L.).

■ REFERENCES

(1) Harvey, A. L.; Edrada-Ebel, R.; Quinn, R. J. The re-emergence of natural products for drug discovery in the genomics era. *Nat. Rev. Drug Discovery* **2015**, *14*, 111−129.
(2) Atanasov, A. G.; Zotchev, S. B.; Supuran, C. T.; the International Natural Product Sciences, T.. Natural products in drug discovery: advances and opportunities. *Nat. Rev. Drug Discovery* **2021**, *20*, 200−216.
(3) Newman, D. J.; Cragg, G. M. Natural Products as Sources of New Drugs from 1981 to 2014. *J. Nat. Prod.* **2016**, *79*, 629−661.
(4) Young, R. J.; Flitsch, S. L.; Grigalunas, M.; Leeson, P. D.; Quinn, R. J.; Turner, N. J.; Waldmann, H. The Time and Place for Nature in Drug Discovery. *JACS Au* **2022**, *2*, 2400−2416.
(5) Walsh, C. T.; Fischbach, M. A. Natural Products Version 2.0: Connecting Genes to Molecules. *J. Am. Chem. Soc.* **2010**, *132*, 2469−2493.
(6) Liu, J.; Xie, X.; Li, S.-M. Increasing cytochrome P450 enzyme diversity by identification of two distinct cyclodipeptide dimerases. *Chem. Commun.* **2020**, *56*, 11042−11045.
(7) García-Domínguez, P.; Areal, A.; Alvarez, R.; de Lera, A. R. Chemical synthesis in competition with global genome mining and heterologous expression for the preparation of dimeric tryptophan-derived 2,5-dioxopiperazines. *Nat. Prod. Rep.* **2022**, *39*, 1172−1225.
(8) Sun, C.; Tian, W.; Lin, Z.; Qu, X. Biosynthesis of pyrroloindoline-containing natural products. *Nat. Prod. Rep.* **2022**, *39*, 1721−1765.
(9) Barra, L.; Awakawa, T.; Abe, I. Noncanonical Functions of Enzyme Cofactors as Building Blocks in Natural Product Biosynthesis. *JACS Au* **2022**, *2*, 1950−1963.
(10) Borthwick, A. D. 2,5-Diketopiperazines: Synthesis, Reactions, Medicinal Chemistry, and Bioactive Natural Products. *Chem. Rev.* **2012**, *112*, 3641−3716.
(11) Ma, Y.-M.; Liang, X.-A.; Kong, Y.; Jia, B. Structural Diversity and Biological Activities of Indole Diketopiperazine Alkaloids from Fungi. *J. Agric. Food Chem.* **2016**, *64*, 6659−6671.
(12) Buedenbender, L.; Grkovic, T.; Duffy, S.; Kurtböke, D. I.; Avery, V. M.; Carroll, A. R. Naseseazine C, a new anti-plasmodial dimeric diketopiperazine from a marine sediment derived Streptomyces sp. *Tetrahedron Lett.* **2016**, *57*, 5893−5895.
(13) Tian, W.; Sun, C.; Zheng, M.; Harmer, J. R.; Yu, M.; Zhang, Y.; Peng, H.; Zhu, D.; Deng, Z.; Chen, S.-L.; Mobli, M.; Jia, X.; Qu, X. Efficient biosynthesis of heterodimeric C3-aryl pyrroloindoline alkaloids. *Nat. Commun.* **2018**, *9*, No. 4428.
(14) Stierle, S. A.; Harken, L.; Li, S.-M. Production of Diketopiperazine Derivatives by Pathway Engineering with Different Cyclodipeptide Synthases from Various Streptomyces Strains. *ACS Synth. Biol.* **2023**, *12*, 1804−1812.
(15) Denisov, I. G.; Makris, T. M.; Sligar, S. G.; Schlichting, I. Structure and Chemistry of Cytochrome P450. *Chem. Rev.* **2005**, *105*, 2253−2278.
(16) Ortiz de Montellano, P. R. Hydrocarbon Hydroxylation by Cytochrome P450 Enzymes. *Chem. Rev.* **2010**, *110*, 932−948.
(17) Zhang, X.; Li, S. Expansion of chemical space for natural products by uncommon P450 reactions. *Nat. Prod. Rep.* **2017**, *34*, 1061−1089.
(18) Li, R.-J.; Tian, K.; Li, X.; Gaikaiwari, A. R.; Li, Z. Engineering P450 Monooxygenases for Highly Regioselective and Active p-Hydroxylation of m-Alkylphenols. *ACS Catal.* **2022**, *12*, 5939−5948.
(19) Tavanti, M.; Porter, J. L.; Sabatini, S.; Turner, N. J.; Flitsch, S. L. Panel of New Thermostable CYP116B Self-Sufficient Cytochrome P450 Monooxygenases that Catalyze C−H Activation with a Diverse Substrate Scope. *ChemCatChem* **2018**, *10*, 1042−1051.
(20) Manning, J.; Tavanti, M.; Porter, J. L.; Kress, N.; De Visser, S. P.; Turner, N. J.; Flitsch, S. L. Regio- and Enantio-selective Chemoenzymatic C−H-Lactonization of Decanoic Acid to (S)-δ-Decalactone. *Angew. Chem., Int. Ed.* **2019**, *58*, 5668−5671.
(21) Dubey, K. D.; Shaik, S. Cytochrome P450−The Wonderful Nanomachine Revealed through Dynamic Simulations of the Catalytic Cycle. *Acc. Chem. Res.* **2019**, *52*, 389−399.
(22) Shaik, S.; Dubey, K. D. Nanomachines in living matters: the soft-robot cytochrome P450. *Trends Chem.* **2023**, *5*, 763−774.
(23) Zhang, X.; Shen, P.; Zhao, J.; Chen, Y.; Li, X.; Huang, J.-W.; Zhang, L.; Li, Q.; Gao, C.; Xing, Q.; Chen, C.-C.; Guo, R.-T.; Li, A. Rationally Controlling Selective Steroid Hydroxylation via Scaffold Sampling of a P450 Family. *ACS Catal.* **2023**, *13*, 1280−1289.
(24) Liu, J.; Harken, L.; Yang, Y.; Xie, X.; Li, S.-M. Widely Distributed Bifunctional Bacterial Cytochrome P450 Enzymes Catalyze both Intramolecular C−C Bond Formation in cyclo-l-Tyr-l-Tyr and Its Coupling with Nucleobases. *Angew. Chem., Int. Ed.* **2022**, *61*, No. e202200377, DOI: 10.1002/anie.202200377.
(25) Harken, L.; Li, S.-M. Modifications of diketopiperazines assembled by cyclodipeptide synthases with cytochrome P450 enzymes. *Appl. Microbiol. Biotechnol.* **2021**, *105*, 2277−2285.
(26) Sun, C.; Ma, B.-D.; Li, G.; Tian, W.; Yang, L.; Peng, H.; Lin, Z.; Deng, Z.; Kong, X.-D.; Qu, X. Engineering the Substrate Specificity of a P450 Dimerase Enables the Collective Biosynthesis of Heterodimeric Tryptophan-Containing Diketopiperazines. *Angew. Chem., Int. Ed.* **2023**, *135*, No. e202304994, DOI: 10.1002/ange.202304994.
(27) Shende, V. V.; Khatri, Y.; Newmister, S. A.; Sanders, J. N.; Lindovska, P.; Yu, F.; Doyon, T. J.; Kim, J.; Houk, K. N.; Movassaghi, M.; Sherman, D. H. Structure and Function of NzeB, a Versatile C-C and C-N Bond-Forming Diketopiperazine Dimerase. *J. Am. Chem. Soc.* **2020**, *142*, 17413−17424.
(28) Sun, C.; Luo, Z.; Zhang, W.; Tian, W.; Peng, H.; Lin, Z.; Deng, Z.; Kobe, B.; Jia, X.; Qu, X. Molecular basis of regio- and stereospecificity in biosynthesis of bacterial heterodimeric diketopiperazines. *Nat. Commun.* **2020**, *11*, No. 6251.
(29) Shende, V. V.; Harris, N. R.; Sanders, J. N.; Newmister, S. A.; Khatri, Y.; Movassaghi, M.; Houk, K. N.; Sherman, D. H. Molecular Dynamics Simulations Guide Chimeragenesis and Engineered Control of Chemoselectivity in Diketopiperazine Dimerases. *Angew. Chem., Int. Ed.* **2023**, *62*, No. e202210254.
(30) Cai, S.; Sun, S.; Peng, J.; Kong, X.; Zhou, H.; Zhu, T.; Gu, Q.; Li, D. Okaramines S−U, three new indole diketopiperazine alkaloids from Aspergillus taichungensis ZHN-7−07. *Tetrahedron* **2015**, *71*, 3715−3719.
(31) Hüttel, W.; Müller, M. Regio- and stereoselective intermolecular phenol coupling enzymes in secondary metabolite biosynthesis. *Nat. Prod. Rep.* **2021**, *38*, 1011−1043.
(32) Liu, J.; Liu, A.; Hu, Y. Enzymatic dimerization in the biosynthetic pathway of microbial natural products. *Nat. Prod. Rep.* **2021**, *38*, 1469−1505.
(33) Zhang, X.; Guo, J.; Cheng, F.; Li, S. Cytochrome P450 enzymes in fungal natural product biosynthesis. *Nat. Prod. Rep.* **2021**, *38*, 1072−1099.
(34) Ushimaru, R.; Abe, I. C−N and C−S bond formation by cytochrome P450 enzymes. *Trends Chem.* **2023**, *5*, 526−536.
(35) Sheng, X.; Zhang, H.; Im, S.-C.; Horner, J. H.; Waskell, L.; Hollenberg, P. F.; Newcomb, M. Kinetics of Oxidation of Benzphetamine by Compounds I of Cytochrome P450 2B4 and Its Mutants. *J. Am. Chem. Soc.* **2009**, *131*, 2971−2976.

(36) Rittle, J.; Green, M. T. Cytochrome P450 Compound I: Capture, Characterization, and C-H Bond Activation Kinetics. *Science* **2010**, *330*, 933−937.
(37) Shaik, S.; Cohen, S.; Wang, Y.; Chen, H.; Kumar, D.; Thiel, W. P450 Enzymes: Their Structure, Reactivity, and Selectivity−Modeled by QM/MM Calculations. *Chem. Rev.* **2010**, *110*, 949−1017.
(38) Nguyen, R. C.; Davis, I.; Dasgupta, M.; Wang, Y.; Simon, P. S.; Butryn, A.; Makita, H.; Bogacz, I.; Dornevil, K.; Aller, P.; Bhowmick, A.; Chatterjee, R.; Kim, I.-S.; Zhou, T.; Mendez, D.; Paley, D. W.; Fuller, F.; Alonso Mori, R.; Batyuk, A.; Sauter, N. K.; Brewster, A. S.; Orville, A. M.; Yachandra, V. K.; Yano, J.; Kern, J. F.; Liu, A. In Situ Structural Observation of a Substrate- and Peroxide-Bound High-Spin Ferric-Hydroperoxo Intermediate in the P450 Enzyme CYP121. *J. Am. Chem. Soc.* **2023**, *145*, 25120−25133.
(39) Fielding, A. J.; Dornevil, K.; Ma, L.; Davis, I.; Liu, A. Probing Ligand Exchange in the P450 Enzyme CYP121 from Mycobacterium tuberculosis: Dynamic Equilibrium of the Distal Heme Ligand as a Function of pH and Temperature. *J. Am. Chem. Soc.* **2017**, *139*, 17484−17499.
(40) Chuanprasit, P.; Goh, S. H.; Hirao, H. Benzyne Formation in the Mechanism-Based Inactivation of Cytochrome P450 by 1-Aminobenzotriazole and N-Benzyl-1-Aminobenzotriazole: Computational Insights. *ACS Catal.* **2015**, *5*, 2952−2960.
(41) Ahmadi, S.; Barrios Herrera, L.; Chehelamirani, M.; Hostaš, J.; Jalife, S.; Salahub, D. R. Multiscale modeling of enzymes: QM-cluster, QM/MM, and QM/MM/MD: A tutorial review. *Int. J. Quantum Chem.* **2018**, *118*, No. e25558.
(42) Ojeda-May, P.; Mushtaq, A. U. I.; Rogne, P.; Verma, A.; Ovchinnikov, V.; Grundström, C.; Dulko-Smith, B.; Sauer, U. H.; Wolf-Watz, M.; Nam, K. Dynamic Connection between Enzymatic Catalysis and Collective Protein Motions. *Biochemistry* **2021**, *60*, 2246−2258.
(43) Sahil, M.; Singh, T.; Ghosh, S.; Mondal, J. 3site Multisubstrate-Bound State of Cytochrome P450cam. *J. Am. Chem. Soc.* **2023**, *145*, 23488−23502.
(44) Shaik, S.; Kumar, D.; de Visser, S. P.; Altun, A.; Thiel, W. Theoretical Perspective on the Structure and Mechanism of Cytochrome P450 Enzymes. *Chem. Rev.* **2005**, *105*, 2279−2328.
(45) Wang, Z.; Diao, W.; Wu, P.; Li, J.; Fu, Y.; Guo, Z.; Cao, Z.; Shaik, S.; Wang, B. How the Conformational Movement of the Substrate Drives the Regioselective C-N Bond Formation in P450 TleB: Insights from Molecular Dynamics Simulations and Quantum Mechanical/Molecular Mechanical Calculations. *J. Am. Chem. Soc.* **2023**, *145*, 7252−7267.
(46) Peng, W.; Yan, S.; Zhang, X.; Liao, L.; Zhang, J.; Shaik, S.; Wang, B. How Do Preorganized Electric Fields Function in Catalytic Cycles? The Case of the Enzyme Tyrosine Hydroxylase. *J. Am. Chem. Soc.* **2022**, *144*, 20484−20494, DOI: 10.1021/jacs.2c09263.
(47) Jiang, Y.; Ding, N.; Shao, Q.; Stull, S. L.; Cheng, Z.; Yang, Z. J. Substrate Positioning Dynamics Involves a Non-Electrostatic Component to Mediate Catalysis. *J. Phys. Chem. Lett.* **2023**, *14*, 11480−11489.
(48) Wang, B.; Wu, P.; Shaik, S. Critical Roles of Exchange and Superexchange Interactions in Dictating Electron Transfer and Reactivity in Metalloenzymes. *J. Phys. Chem. Lett.* **2022**, *13*, 2871−2877.
(49) Wang, B.; Zhang, X.; Fang, W.; Rovira, C.; Shaik, S. How Do Metalloproteins Tame the Fenton Reaction and Utilize •OH Radicals in Constructive Manners? *Acc. Chem. Res.* **2022**, *55*, 2280−2290.
(50) Ye, Y.; Du, L.; Zhang, X.; Newmister, S. A.; McCauley, M.; Alegre-Requena, J. V.; Zhang, W.; Mu, S.; Minami, A.; Fraley, A. E.; Adrover-Castellano, M. L.; Carney, N. A.; Shende, V. V.; Qi, F.; Oikawa, H.; Kato, H.; Tsukamoto, S.; Paton, R. S.; Williams, R. M.; Sherman, D. H.; Li, S. Fungal-derived brevianamide assembly by a stereoselective semipinacolase. *Nat. Catal.* **2020**, *3*, 497−506.
(51) Cao, Y.-C.; Liao, R.-Z. QM Calculations Revealed that Outer-Sphere Electron Transfer Boosted O−O Bond Cleavage in the Multiheme-Dependent Cytochrome bd Oxygen Reductase. *Inorg. Chem.* **2023**, *62*, 4066−4075.
(52) Hu, R.; Gong, A.; Liao, L.; Zheng, Y.-X.; Liu, X.; Wu, P.; Li, F.; Yu, H.; Zhao, J.; Ye, L.-W.; Wang, B.; Li, A. Biocatalytic aminohydroxylation of styrenes for efficient synthesis of enantiopure *β*-amino alcohols. *Chin. J. Catal.* **2023**, *44*, 171−178.
(53) Salomon-Ferrer, R.; Case, D. A.; Walker, R. C. An overview of the Amber biomolecular simulation package. *Wiley Interdiscip. Rev.: Comput. Mol. Sci.* **2013**, *3*, 198−210, DOI: 10.1002/wcms.1121.
(54) Yue, D.; Hirao, H. Mechanism of Selective Aromatic Hydroxylation in the Metabolic Transformation of Paclitaxel Catalyzed by Human CYP3A4. *J. Chem. Inf. Model.* **2023**, *63*, 7826−7836.
(55) Senn, H. M.; Thiel, W. QM/MM Methods for Biomolecular Systems. *Angew. Chem., Int. Ed.* **2009**, *48*, 1198−1229.
(56) van der Kamp, M. W.; Mulholland, A. J. Combined quantum mechanics/molecular mechanics (QM/MM) methods in computational enzymology. *Biochemistry* **2013**, *52*, 2708−2728.
(57) Metz, S.; Kästner, J.; Sokol, A. A.; Keal, T. W.; Sherwood, P. ChemShell−a modular software package for QM/MM simulations. *Wiley Interdiscip. Rev.: Comput. Mol. Sci.* **2014**, *4*, 101−110, DOI: 10.1002/wcms.1163.
(58) Xu, K.; Wang, Y.; Hirao, H. Estrogen Formation via H-Abstraction from the O−H Bond of gem-Diol by Compound I in the Reaction of CYP19A1: Mechanistic Scenario Derived from Multiscale QM/MM Calculations. *ACS Catal.* **2015**, *5*, 4175−4179.
(59) Li, A.; Wang, B.; Ilie, A.; Dubey, K. D.; Bange, G.; Korendovych, I. V.; Shaik, S.; Reetz, M. T. A redox-mediated Kemp eliminase. *Nat. Commun.* **2017**, *8*, No. 14876.
(60) Fiser, A.; Šali, A. Modeller: Generation and Refinement of Homology-Based Protein Structure Models. *Methods Enzymol.* **2003**, *374*, 461−491.
(61) Siddiqui, S. A.; Stuyver, T.; Shaik, S.; Dubey, K. D. Designed Local Electric Fields—Promising Tools for Enzyme Engineering. *JACS Au* **2023**, *3*, 3259−3269.
(62) Yadav, S.; Shaik, S.; Dubey, K. D. Decarboxylation and Protonation Enigma in the H85Q Mutant of Cytochrome P450OleT. *J. Phys. Chem. B* **2023**, *127*, 2927−2933.
(63) Søndergaard, C. R.; Olsson, M. H. M.; Rostkowski, M.; Jensen, J. H. Improved Treatment of Ligands and Coupling Effects in Empirical Calculation and Rationalization of pKa Values. *J. Chem. Theory Comput.* **2011**, *7*, 2284−2295.
(64) Olsson, M. H. M.; Søndergaard, C. R.; Rostkowski, M.; Jensen, J. H. PROPKA3: Consistent Treatment of Internal and Surface Residues in Empirical pKa Predictions. *J. Chem. Theory Comput.* **2011**, *7*, 525−537.
(65) Humphrey, W.; Dalke, A.; Schulten, K. VMD: visual molecular dynamics. *J. Mol. Graphics* **1996**, *14*, 33−38.
(66) Case, D. A.; Brozell, S. R.; Cerutti, D. S.; Cheatham, T. E.; Cruzeiro, I. V. W. D.; Darden, T. A.; Duke, R. E.; Ghoreishi, D.; Gilson, M. K.; Gohlke, H.; Goetz, A. W.; Greene, D.; Harris, R.; Homeyer, N.; Izadi, S.; Kovalenko, A.; Kurtzman, T.; Lee, T. S.; LeGrand, S.; Li, P. L. C.; Liu, J.; Luchko, T.; Luo, R.; Mermelstein, D. J.; Merz, K. M.; Miao, Y.; Monard, G.; Nguyen, C.; Nguyen, H.; Omelyan, I.; Onufriev, A.; Pan, F.; Qi, R.; Roe, D. R.; Roitberg, A.; Sagui, C.; Schott-Verdugo, S.; Shen, J.; Simmerling, C. L.; Smith, J.; Salomon-Ferrer, R.; Swails, J.; Walker, R. C.; Wang, J.; Wei, H.; Wolf, R. M.; Wu, X.; Xiao, L.; York, D. M.; Kollman, P. A. *Amber 2018*; University of California: San Francisco, 2018.
(67) Wang, J.; Wolf, R. M.; Caldwell, J. W.; Kollman, P. A.; Case, D. A. Development and testing of a general amber force field. *J. Comput. Chem.* **2004**, *25*, 1157−1174.
(68) Bayly, C. I.; Cieplak, P.; Cornell, W.; Kollman, P. A. A well-behaved electrostatic potential based method using charge restraints for deriving atomic charges: the RESP model. *J. Phys. Chem. A* **1993**, *97*, 10269−10280.
(69) Becke, A. D. Density-functional thermochemistry. III. The role of exact exchange. *J. Chem. Phys.* **1993**, *98*, 5648−5652.
(70) Grimme, S.; Ehrlich, S.; Goerigk, L. Effect of the damping function in dispersion corrected density functional theory. *J. Comput. Chem.* **2011**, *32*, 1456−1465.

(71) Maier, J. A.; Martinez, C.; Kasavajhala, K.; Wickstrom, L.; Hauser, K. E.; Simmerling, C. ff14SB: Improving the Accuracy of Protein Side Chain and Backbone Parameters from ff99SB. *J. Chem. Theory Comput.* **2015**, *11*, 3696−3713.
(72) Shahrokh, K.; Orendt, A.; Yost, G. S.; Cheatham Iii, T. E. Quantum mechanically derived AMBER-compatible heme parameters for various states of the cytochrome P450 catalytic cycle. *J. Comput. Chem.* **2012**, *33*, 119−133.
(73) Li, P.; Merz, K. M. MCPB.py: A Python Based Metal Center Parameter Builder. *J. Chem. Inf. Model.* **2016**, *56*, 599−604.
(74) Li, P.; Merz, K. M., Jr. Metal Ion Modeling Using Classical Mechanics. *Chem. Rev.* **2017**, *117*, 1564−1686.
(75) Jorgensen, W. L.; Chandrasekhar, J.; Madura, J. D.; Impey, R. W.; Klein, M. L. Comparison of simple potential functions for simulating liquid water. *J. Chem. Phys.* **1983**, *79*, 926−935.
(76) Izaguirre, J. A.; Catarello, D. P.; Wozniak, J. M.; Skeel, R. D. Langevin stabilization of molecular dynamics. *J. Chem. Phys.* **2001**, *114*, 2090−2098.
(77) Berendsen, H. J. C.; Postma, J. P. M.; van Gunsteren, W. F.; DiNola, A.; Haak, J. R. Molecular dynamics with coupling to an external bath. *J. Chem. Phys.* **1984**, *81*, 3684−3690.
(78) Kräutler, V.; van Gunsteren, W. F.; Hünenberger, P. H. A fast SHAKE algorithm to solve distance constraint equations for small molecules in molecular dynamics simulations. *J. Comput. Chem.* **2001**, *22*, 501−508.
(79) Lu, Y.; Sen, K.; Yong, C.; Gunn, D. S. D.; Purton, J. A.; Guan, J.; Desmoutier, A.; Abdul Nasir, J.; Zhang, X.; Zhu, L.; Hou, Q.; Jackson-Masters, J.; Watts, S.; Hanson, R.; Thomas, H. N.; Jayawardena, O.; Logsdail, A. J.; Woodley, S. M.; Senn, H. M.; Sherwood, P.; Catlow, C. R. A.; Sokol, A. A.; Keal, T. W. Multiscale QM/MM modelling of catalytic systems with ChemShell. *Phys. Chem. Chem. Phys.* **2023**, *25*, 21816−21835.
(80) Ahlrichs, R.; Bär, M.; Häser, M.; Horn, H.; Kölmel, C. Electronic structure calculations on workstation computers: The program system turbomole. *Chem. Phys. Lett.* **1989**, *162*, 165−169.
(81) Smith, W.; Forester, T. R. DL_POLY_2.0: A general-purpose parallel molecular dynamics simulation package. *J. Mol. Graphics* **1996**, *14*, 136−141.
(82) Smith, W.; Yong, C. W.; Rodger, P. M. DL_POLY: Application to molecular simulation. *Mol. Simul.* **2002**, *28*, 385−471.
(83) Bakowies, D.; Thiel, W. Hybrid Models for Combined Quantum Mechanical and Molecular Mechanical Approaches. *J. Phys. Chem. A* **1996**, *100*, 10580−10594.
(84) Kalita, S.; Shaik, S.; Dubey, K. D. Mechanistic Conundrum of C−C Bond Cleavage by CYP51. *ACS Catal.* **2022**, *12*, 5673−5683.
(85) Kalita, S.; Shaik, S.; Kisan, H. K.; Dubey, K. D. A Paradigm Shift in the Catalytic Cycle of P450: The Preparatory Choreography during O2 Binding and Origins of the Necessity for Two Protonation Pathways. *ACS Catal.* **2020**, *10*, 11481−11492.
(86) Yang, Y.; Cho, I.; Qi, X.; Liu, P.; Arnold, F. H. An enzymatic platform for the asymmetric amination of primary, secondary and tertiary C(sp3)−H bonds. *Nat. Chem.* **2019**, *11*, 987−993.
(87) Zhang, X.; Jiang, Y.; Chen, Q.; Dong, S.; Feng, Y.; Cong, Z.; Shaik, S.; Wang, B. H-Bonding Networks Dictate the Molecular Mechanism of H2O2 Activation by P450. *ACS Catal.* **2021**, *11*, 8774−8785.
(88) Zhang, S.; Li, X.; Wang, Y.; Wei, J.; Zhang, X.; Liu, Y. Computational Study of the Peroxygenase Mechanism Catalyzed by Hemoglobin Dehaloperoxidase Involved in the Degradation of Chlorophenols. *Inorg. Chem.* **2022**, *61*, 2628−2639.
(89) Schäfer, A.; Horn, H.; Ahlrichs, R. Fully optimized contracted Gaussian basis sets for atoms Li to Kr. *J. Chem. Phys.* **1992**, *97*, 2571−2577.
(90) Henkelman, G.; Jónsson, H. A dimer method for finding saddle points on high dimensional potential surfaces using only first derivatives. *J. Chem. Phys.* **1999**, *111*, 7010−7022.
(91) Kästner, J.; Carr, J. M.; Keal, T. W.; Thiel, W.; Wander, A.; Sherwood, P. DL-FIND: An Open-Source Geometry Optimizer for Atomistic Simulations. *J. Phys. Chem. A* **2009**, *113*, 11856−11865.
(92) Gergel, S.; Soler, J.; Klein, A.; Schülke, K. H.; Hauer, B.; Garcia-Borràs, M.; Hammer, S. C. Engineered cytochrome P450 for direct arylalkene-to-ketone oxidation via highly reactive carbocation intermediates. *Nat. Catal.* **2023**, *6*, 606−617.
(93) Haas, J.; Beck, E.; Troczka, B. J.; Hayward, A.; Hertlein, G.; Zaworra, M.; Lueke, B.; Buer, B.; Maiwald, F.; Beck, M. E.; Nebelsiek, B.; Glaubitz, J.; Bass, C.; Nauen, R. A conserved hymenopteran-specific family of cytochrome P450s protects bee pollinators from toxic nectar alkaloids. *Sci. Adv.* **2023**, *9*, No. eadg0885.
(94) Santos, S. F. G.; Bommareddy, R. R.; Black, G. W.; Singh, W.; Huang, M. The substrate specificity in the O-demethylation of 4-alkylguaiacols by cytochrome P450 AgcAP450. *Catal. Sci. Technol.* **2023**, *13*, 2070−2079.
(95) Wei, J.; Liu, Y. Mechanistic Insights into the P450 TleB-Catalyzed Unusual Intramolecular C−N Bond Formation Involved in the Biosynthesis of Indolactam V. *J. Chem. Inf. Model.* **2021**, *61*, 3638−3648.
(96) Visser, P. d. S.; Porro, S. C.; Quesne, G. M.; Sainna, A. M.; Munro, W. A. Overview on Theoretical Studies Discriminating the Two-Oxidant Versus Two-State-Reactivity Models for Substrate Monoxygenation by Cytochrome P450 Enzymes. *Curr. Top. Med. Chem.* **2013**, *13*, 2218−2232.
(97) Louka, S.; Barry, S. M.; Heyes, D. J.; Mubarak, M. Q. E.; Ali, H. S.; Alkhalaf, L. M.; Munro, A. W.; Scrutton, N. S.; Challis, G. L.; de Visser, S. P. Catalytic Mechanism of Aromatic Nitration by Cytochrome P450 TxtE: Involvement of a Ferric-Peroxynitrite Intermediate. *J. Am. Chem. Soc.* **2020**, *142*, 15764−15779.
(98) Chen, H.; Zhou, A.; Sun, D.; Zhao, Y.; Wang, Y. Theoretical Investigation on the Elusive Reaction Mechanism of Spirooxindole Formation Mediated by Cytochrome P450s: A Nascent Feasible Charge-Shift C−O Bond Makes a Difference. *J. Phys. Chem. B* **2021**, *125*, 8419−8430.
(99) Torrie, G. M.; Valleau, J. P. Nonphysical sampling distributions in Monte Carlo free-energy estimation: Umbrella sampling. *J. Comput. Phys.* **1977**, *23*, 187−199.
(100) Kumar, S.; Rosenberg, J. M.; Bouzida, D.; Swendsen, R. H.; Kollman, P. A. THE weighted histogram analysis method for free-energy calculations on biomolecules. I. The method. *J. Comput. Chem.* **1992**, *13*, 1011−1021.
(101) Souaille, M.; Roux, Bt. Extension to the weighted histogram analysis method: combining umbrella sampling with free energy calculations. *Comput. Phys. Commun.* **2001**, *135*, 40−57.
(102) Kalita, S.; Shaik, S.; Dubey, K. D. MD simulations and QM/MM calculations reveal the key mechanistic elements which are responsible for the efficient C−H amination reaction performed by a bioengineered P450 enzyme. *Chem. Sci.* **2021**, *12*, 14507−14518.
(103) Fang, W.; Feng, S.; Jiang, Z.; Liang, W.; Li, P.; Wang, B. Understanding the Key Roles of pH Buffer in Accelerating Lignin Degradation by Lignin Peroxidase. *JACS Au* **2023**, *3*, 536−549.
(104) Pliego, J. R. Thermodynamic cycles and the calculation of pKa. *Chem. Phys. Lett.* **2003**, *367*, 145−149.
(105) Poulos, T. L. Cytochrome P450 flexibility. *Proc. Natl. Acad. Sci. U.S.A.* **2003**, *100*, 13121−13122.
(106) Skopalík, J.; Anzenbacher, P.; Otyepka, M. Flexibility of Human Cytochromes P450: Molecular Dynamics Reveals Differences between CYPs 3A4, 2C9, and 2A6, which Correlate with Their Substrate Preferences. *J. Phys. Chem. B* **2008**, *112*, 8165−8173.
(107) Sevrioukova, I. F.; Poulos, T. L. Structural basis for regiospecific midazolam oxidation by human cytochrome P450 3A4. *Proc. Natl. Acad. Sci. U.S.A.* **2017**, *114*, 486−491.
(108) Yang, Y.; Wong, S. E.; Lightstone, F. C. Understanding a Substrate's Product Regioselectivity in a Family of Enzymes: A Case Study of Acetaminophen Binding in Cytochrome P450s. *PLoS One* **2014**, *9*, No. e87058.
(109) Cui, G.; Merz, K. M. Computational Studies of the Farnesyltransferase Ternary Complex Part II: The Conformational Activation of Farnesyldiphosphate. *Biochemistry* **2007**, *46*, 12375−12381.

https://doi.org/10.1021/jacsau.4c00075
JACS Au 2024, 4, 1591−1604

(110) Wang, Z.; Shaik, S.; Wang, B. Conformational Motion of Ferredoxin Enables Efficient Electron Transfer to Heme in the Full-Length P450TT. *J. Am. Chem. Soc.* **2021**, *143*, 1005−1016.
(111) Wu, P.; Fan, F.; Song, J.; Peng, W.; Liu, J.; Li, C.; Cao, Z.; Wang, B. Theory Demonstrated a ″Coupled″ Mechanism for O2 Activation and Substrate Hydroxylation by Binuclear Copper Monooxygenases. *J. Am. Chem. Soc.* **2019**, *141*, 19776−19789.
(112) Adasme, M. F.; Linnemann, K. L.; Bolz, S. N.; Kaiser, F.; Salentin, S.; Haupt, V. J.; Schroeder, M. PLIP 2021: expanding the scope of the protein−ligand interaction profiler to DNA and RNA. *Nucleic Acids Res.* **2021**, *49*, W530−W534.
(113) Gering, H. E.; Li, X.; Tang, H.; Swartz, P. D.; Chang, W.-C.; Makris, T. M. A Ferric-Superoxide Intermediate Initiates P450-Catalyzed Cyclic Dipeptide Dimerization. *J. Am. Chem. Soc.* **2023**, *145*, 19256−19264.
(114) Wang, D.; Thiel, W. The oxyheme complexes of P450cam: A QM/MM study. *J. Mol. Struct.: THEOCHEM* **2009**, *898*, 90−96.
(115) Lai, W.; Shaik, S. Can Ferric-Superoxide Act as a Potential Oxidant in P450cam? QM/MM Investigation of Hydroxylation, Epoxidation, and Sulfoxidation. *J. Am. Chem. Soc.* **2011**, *133*, 5444−5452.
(116) Jonsson, M.; Lind, J.; Eriksen, T. E.; Merenyi, G. Redox and Acidity Properties of 4-Substituted Aniline Radical Cations in Water. *J. Am. Chem. Soc.* **1994**, *116*, 1423−1427.
(117) Shaik, S.; Kumar, D.; de Visser, S. P. A Valence Bond Modeling of Trends in Hydrogen Abstraction Barriers and Transition States of Hydroxylation Reactions Catalyzed by Cytochrome P450 Enzymes. *J. Am. Chem. Soc.* **2008**, *130*, 10128−10140.
(118) Dey, A.; Okamura, T.-a.; Ueyama, N.; Hedman, B.; Hodgson, K. O.; Solomon, E. I. Sulfur K-Edge XAS and DFT Calculations on P450 Model Complexes: Effects of Hydrogen Bonding on Electronic Structure and Redox Potentials. *J. Am. Chem. Soc.* **2005**, *127*, 12046−12053.
(119) Zhang, Y.; Mokkawes, T.; de Visser, S. P. Insights into Cytochrome P450 Enzyme Catalyzed Defluorination of Aromatic Fluorides. *Angew. Chem., Int. Ed.* **2023**, *62*, No. e202310785, DOI: 10.1002/anie.202310785.
(120) Kim, H.; Rogler, P. J.; Sharma, S. K.; Schaefer, A. W.; Solomon, E. I.; Karlin, K. D. Heme-FeIII Superoxide, Peroxide and Hydroperoxide Thermodynamic Relationships: FeIII-O2•− Complex H-Atom Abstraction Reactivity. *J. Am. Chem. Soc.* **2020**, *142*, 3104−3116.
(121) Zaragoza, J. P. T.; Cummins, D. C.; Mubarak, M. Q. E.; Siegler, M. A.; de Visser, S. P.; Goldberg, D. P. Hydrogen Atom Abstraction by High-Valent Fe(OH) versus Mn(OH) Porphyrinoid Complexes: Mechanistic Insights from Experimental and Computational Studies. *Inorg. Chem.* **2019**, *58*, 16761−16770.
(122) Davis, J. A.; Greene, R. J.; Han, S.; Rock, D. A.; Wienkers, L. C. Formation of raloxifene homo-dimer in CYP3A4, evidence for multi-substrate binding in a single catalytically competent P450 active site. *Arch. Biochem. Biophys.* **2011**, *513*, 110−118.
(123) Lin, H.-C.; McMahon, T. C.; Patel, A.; Corsello, M.; Simon, A.; Xu, W.; Zhao, M.; Houk, K. N.; Garg, N. K.; Tang, Y. P450-Mediated Coupling of Indole Fragments To Forge Communesin and Unnatural Isomers. *J. Am. Chem. Soc.* **2016**, *138*, 4002−4005.
(124) Li, C.; Hu, Y.; Wu, X.; Stumpf, S. D.; Qi, Y.; D'Alessandro, J. M.; Nepal, K. K.; Sarotti, A. M.; Cao, S.; Blodgett, J. A. V. Discovery of unusual dimeric piperazyl cyclopeptides encoded by a Lentzea flaviverrucosa DSM 44664 biosynthetic supercluster. *Proc. Natl. Acad. Sci. U.S.A.* **2022**, *119*, No. e2117941119.
(125) Chang, Y.; Zhou, L.; Hou, X.; Zhu, T.; Pfeifer, B. A.; Li, D.; He, X.; Zhang, G.; Che, Q. Microbial Dimerization and Chlorination of Isoflavones by a Takla Makan Desert-Derived Streptomyces sp. HDN154127. *J. Nat. Prod.* **2023**, *86*, 34−44.
(126) Guo, Z.; Li, P.; Chen, G.; Li, C.; Cao, Z.; Zhang, Y.; Ren, J.; Xiang, H.; Lin, S.; Ju, J.; Chen, Y. Design and Biosynthesis of Dimeric Alboflavusins with Biaryl Linkages via Regiospecific C−C Bond Coupling. *J. Am. Chem. Soc.* **2018**, *140*, 18009−18015.
(127) Guengerich, F. P.; Yoshimoto, F. K. Formation and Cleavage of C−C Bonds by Enzymatic Oxidation−Reduction Reactions. *Chem. Rev.* **2018**, *118*, 6573−6655.
(128) He, F.; Mori, T.; Morita, I.; Nakamura, H.; Alblova, M.; Hoshino, S.; Awakawa, T.; Abe, I. Molecular basis for the P450-catalyzed C−N bond formation in indolactam biosynthesis. *Nat. Chem. Biol.* **2019**, *15*, 1206−1213.
(129) Mai, B. K.; Neris, N. M.; Yang, Y.; Liu, P. C−N Bond Forming Radical Rebound Is the Enantioselectivity-Determining Step in P411-Catalyzed Enantioselective C(sp3)−H Amination: A Combined Computational and Experimental Investigation. *J. Am. Chem. Soc.* **2022**, *144*, 11215−11225.
(130) Ye, Y.; Minami, A.; Igarashi, Y.; Izumikawa, M.; Umemura, M.; Nagano, N.; Machida, M.; Kawahara, T.; Shin-ya, K.; Gomi, K.; Oikawa, H. Unveiling the Biosynthetic Pathway of the Ribosomally Synthesized and Post-translationally Modified Peptide Ustiloxin B in Filamentous Fungi. *Angew. Chem., Int. Ed.* **2016**, *55*, 8072−8075.
(131) Dunbar, K. L.; Scharf, D. H.; Litomska, A.; Hertweck, C. Enzymatic Carbon−Sulfur Bond Formation in Natural Product Biosynthesis. *Chem. Rev.* **2017**, *117*, 5521−5577.
(132) Morita, I.; Mori, T.; Mitsuhashi, T.; Hoshino, S.; Taniguchi, Y.; Kikuchi, T.; Nagae, K.; Nasu, N.; Fujita, M.; Ohwada, T.; Abe, I. Exploiting a C−N Bond Forming Cytochrome P450 Monooxygenase for C−S Bond Formation. *Angew. Chem., Int. Ed.* **2020**, *59*, 3988−3993.
(133) Klein, A. P.; Sattely, E. S. Two cytochromes P450 catalyze S-heterocyclizations in cabbage phytoalexin biosynthesis. *Nat. Chem. Biol.* **2015**, *11*, 837−839.

https://doi.org/10.1021/jacsau.4c00075
JACS Au 2024, 4, 1591−1604